A Simple Approach to Lattice Effects in Conducting Perovskite-Type Oxides

J. Paul Attfield

Department of Chemistry, University of Cambridge, Lensfield Road, Cambridge CB2 1EW, and Interdisciplinary Research Centre in Superconductivity, University of Cambridge, Madingley Road, Cambridge CB3 0HE, United Kingdom

Received April 1, 1998. Revised Manuscript Received July 2, 1998

A method for parametrizing the A cation size disparity or mismatch in ATO_3 perovskites through the A cation size variance has recently been proposed and experimental studies are reviewed. (A is a mixture of trivalent lanthanide and divalent alkaline-earth cations.) The metal−insulator transition temperature in $AMnO_3$ perovskites and the critical temperature in A_2CuO_4 superconductors are both found to decrease linearly with this size variance at constant doping level and average A cation radius. This result enables a pair of quadratic relationships for the mean size and size variance effects to be proposed as the result of changing strain energies associated with small structural distortions at the electronic transitions. Doping level, mean A cation radius, and the size variance are thus the three major parameters that control electronic properties in oxygen stoichiometric perovskite oxides.

Contents

1. Introduction

Perovskite-type and related oxides of the first row transition metals (T) have long been of interest for their electronic and many other properties.[1,2] All the metals T = Ti−Cu can give rise to metallic conductivity in perovskite-type or related oxides, and metal-to-insulator transitions can be observed in most cases as a function of temperature, pressure, or small chemical changes. More exotic conductivity is also found, most notably, superconductivity in copper oxides[3] and the ferromagnetic metallic state in manganese oxide perovskites associated with colossal magnetoresistances.[4]

Relationships between composition, structure, and properties of ATO_3 perovskites (Figure 1) are usually parametrized using the formal oxidation state of the transition metal and the tolerance factor. The oxidation state describes the number of electrons available to fill the energy bands and the tolerance factor, which is defined later, parametrizes structural effects due to the average sizes of the A site and T cations. However, the recent explosion of interest in the manganite perovskites has shown that these two parameters are not enough and that different $AMnO_3$ samples with the same doping level and tolerance factors can have quite different metal−insulator transition temperatures. This information has led us to consider a third factor that has generally been neglected in this field; that is, the effects of disorder due to the disparity or mismatch of individual A cation radii.

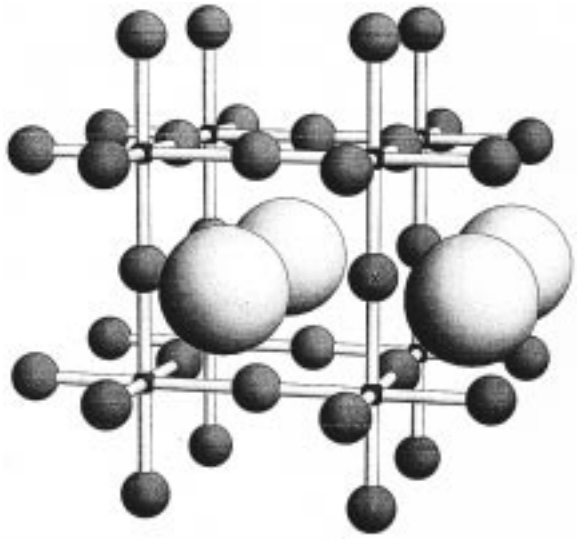

Figure 1. The ideal cubic ATO_3 perovskite structure showing the network of corner-sharing TO_6 octahedra and the four A cations surrounding a given oxygen atom (marked 'x').

Many types of disorder can be present in perovskites, ranging from point vacancies or substitutions to extended features such as shear planes and stacking faults. The simplest to vary and study chemically are point substitutions, such as in $(Ln_{1-x}M_x)TO_3$ compositions (Ln = trivalent lanthanide, M = divalent Ca, Sr, Ba), in which the TO_3 network is stoichiometric and the disorder is easily varied by changing x or substituting other Ln or M cations. This type of disorder is also important because it is needed to induce and tune useful electronic properties, such as the magnetoresistive effect

10.1021/cm980221s CCC: $15.00
Published on Web 10/28/1998

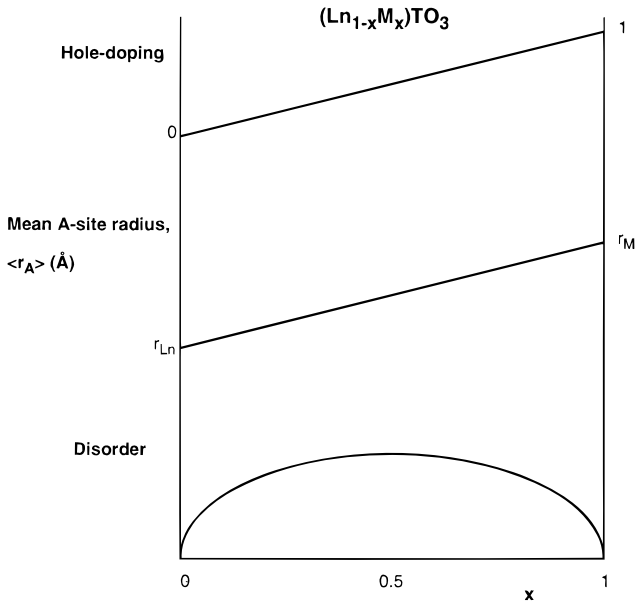

Figure 2. Variation in hole doping, mean cation radius, and size disorder with x in a $(Ln_{1-x}M_x)TO_3$ perovskite.

in $(La_{1-x}Sr_x)MnO_3$ perovskites and superconductivity in $(La_{2-x}Sr_x)CuO_4$, which are absent in the insulating $x = 0$ materials. This review will cover work carried out during the last 2 years on a new approach to the effects of such cation disorder mainly upon electronic transition temperatures T_e. (T_e is the metal−insulator transition temperature, T_m, for $(Ln_{1-x}M_x)MnO_3$ perovskites or the critical temperature, T_c, for $(Ln_{2-x}M_x)CuO_4$ superconductors.)

2. A Cation Substitution Effects in Perovskites

Figure 2 shows the important changes that occur in a $(Ln_{1-x}M_x)TO_3$ perovskite as x is altered. The first two effects are well known. The electron (or hole) concentration, equivalent to the T oxidation state, changes linearly and is the primary cause of changes in electronic behavior because the Ln^{3+} and M^{2+} ions do not contribute to the states around the Fermi level. Insulating behavior is usually found close to 0 and 1 (and other fractional values of x such as 1/2 if charge ordering occurs),[4] with more conducting, often metallic, phases between. However, the exact details vary considerably from one transition metal to another.

The mean A cation radius $\langle r_A \rangle$ also changes linearly with x between the values for the individual cations, for which standard values are available.[5] Ln^{3+} and M^{2+} are assumed to behave as hard, spherical, cations. The average size effect is usually described by the dimensionless perovskite tolerance factor t:

$$t = (\langle r_A \rangle + r_O)/\sqrt{2}(r_T + r_O) \quad (1)$$

where r_O and r_T are the radii of the oxide and transition metal ions, respectively. Stable perovskite materials generally lie in the range $0.8 < t < 1$, with near cubic structures (often rhombohedrally distorted) close to $t = 1$, and more distorted superstructures such as the orthorhombic $GdFeO_3$ type[6] at smaller t values. The distortions usually result in bending of the T−O−T bridges. Both $\langle r_A \rangle$ and r_T change linearly with x (assuming a linear variation in T cation radius with oxidation state); however, $t(x)$ is not linear and so it is more useful here to describe the mean size effect in terms of the average A cation radius $\langle r_A \rangle$.

The amount of structural disorder due to the pseudorandom distribution of A cations with different radii (the 'size disparity' or 'mismatch' effect) also changes with x. This disorder has not usually been studied and there is no widely accepted quantity to parametrize the disorder. We have used the statistical variance in the distribution of radii, $\sigma^2(r_A)$, written as σ^2 throughout this review. In general this variance is defined as

$$\sigma^2 = \sum_i y_i r_i^2 - (\sum_i y_i r_i)^2 \quad (2)$$

$$= \langle r_A^2 \rangle - \langle r_A \rangle^2 \quad (3)$$

The variance (also known as the second moment) is the difference between the mean squared value and the square of the mean and is defined for any number of ions present by the summations in eq 2, where y_i are the proportions of each ion present ($\sum y_i = 1$). When only one type of ion is present, then $\sigma^2 = 0$, and for the mixture of two ions in $(Ln_{1-x}M_x)TO_3$, eq 2 reduces to

$$\sigma^2 = x(1 - x)(\Delta_A)^2 \quad (4)$$

where Δ_A is the difference between the Ln^{3+} and M^{2+} radii. This equation is the quadratic form shown in Figure 2 with a maximum value of $\Delta_A^2/4$ for $x = 0.5$.

3. Experimental Studies

3.1. Correlations between Cation Size Variance and Electronic Transition Temperatures. Section 2 shows that the electron concentration, mean cation size (tolerance factor), and size variance of the $(Ln_{1-x}M_x)TO_3$ perovskite lattice all change with x, and there is no a priori method of estimating or separating their contributions to the changes of the physical property observed. However, by using mixtures of more than two cations at the A sites it is possible in principle to independently change the three variables. Whether it is possible in practice depends on the sizes of available A type cations and whether a homogeneous, oxygen stoichiometric perovskite phase can be synthesized. A number of recent studies have shown that it is possible to vary the size variance while holding the mean doping level and A cation size constant.

(i) $AMnO_3$ Perovskites. There has been much recent interest in doped lanthanide manganese oxide perovskites $(Ln_{1-x}M_x)MnO_3$ because of their colossal magnetoresistances, and fuller descriptions of these materials are given elsewhere.[4,7] A low-temperature ferromagnetic metallic phase often results for $x \approx 0.2-0.5$ from double exchange between localized Mn:t_{2g}^3 configurations mediated by the mobile, spin-polarized e_g electrons hopping from Mn^{3+} to Mn^{4+} ions. As the temperature is raised, a transition to a paramagnetic insulating (semiconducting) state occurs at T_m.

Comparison of the magnetic and electronic phase diagrams for different $AMnO_3$ systems shows that their properties can vary substantially. For example, with $A = (La_{1-x}Sr_x)$, the onset of the ferromagnetic metallic phase is at $x = 0.15$, but for $A = (Pr_{1-x}Sr_x)$, this onset is

Table 1. A Site Compositions of a Series of $(Ln_{0.7}M_{0.3})MnO_3$ Perovskites with a Constant $\langle r_A \rangle$ (1.23 Å) and Increasing Cation Size Variance σ^2 at Various Resistivities ρ_m and Temperatures T_m at the Resistivity Maximum[a]

A site composition[b]	σ^2 (Å^2)	ρ_m (Ω cm)	T_m (K)
$La_{0.70}Ca_{0.11}Sr_{0.19}$ N	0.0016	1.22×10^{-2}	363
$La_{0.32}Pr_{0.38}Sr_{0.30}$ N	0.0029	1.58×10^{-2}	336
$La_{0.53}Sm_{0.17}Sr_{0.30}$	0.0036	1.84×10^{-2}	326
$Pr_{0.70}Sr_{0.23}Ba_{0.07}$ N	0.0074	1.13×10^{-1}	247
$Nd_{0.70}Sr_{0.16}Ba_{0.14}$ N	0.0123	7.96×10^{0}	146
$Nd_{0.41}Sm_{0.29}Ba_{0.20}Sr_{0.10}$	0.0169	9.94×10^{1}	87
$Nd_{0.15}Sm_{0.55}Ba_{0.25}Sr_{0.05}$	0.0207	2.32×10^{2}	76
$Sm_{0.70}Ba_{0.30}$	0.0240	6.67×10^{2}	113

[a] See Figure 3a. [b] Samples marked N were used in the neutron diffraction study described in Section 3.5.

shifted to $x = 0.3$, and in the $(Pr_{1-x}Ca_x)$ system, this state is not observed for any x at ambient pressures.[8] This marked dependence of properties on the A cations used led to the first systematic study of size disparity using the variance as an experimental variable in a series of $(Ln_{0.7}M_{0.3})MnO_3$ perovskites with compositions shown in Table 1.[9] These results illustrate how σ^2 can be increased through the use of progressively smaller lanthanides (La → Pr → Nd → Sm) and larger alkaline earth cations (Ca → Sr → Ba) while keeping the doping level ($x = 0.3$) and the mean size ($\langle r_A \rangle = 1.23$ Å) fixed. Resistivities and magnetization data are shown in Figure 3. The wide range of T_m values (taken from the resistivity maxima in Figure 3a) from ~100 to 360 K in this one series of samples shows that the transition is very sensitive to A cation size disparity. Furthermore, T_m decreases linearly with σ^2 (Figure 4) up to $\sigma^2 \approx 0.015$ Å^2 (above which the samples are inhomogeneous), indicating that there may be a simple physical explanation for this effect.

The linear correlation between T_e (=T_m) and σ^2 is fitted as

$$T_e = T_e^0 - p_1\sigma^2 \qquad (5)$$

where the negative slope p_1 quantifies the size variance dependence of T_e and the intercept T_e^0 (=T_m^0) is an experimental estimate of the ideal transition temperature that would be observed if cation size disorder were not present. The experimentally fitted values of these parameters are given in Table 2.

Another series of six $(Ln_{0.7}M_{0.3})MnO_3$ samples with a larger $\langle r_A \rangle = 1.26$ Å has subsequently been similarly prepared.[10] Their T_m values (Figure 5) also show an approximately linear variation with σ^2. The fitted parameters (Table 2) show that p_1 decreases and T_m^0 increases with $\langle r_A \rangle$.

Linear correlations between T_m and σ^2 were also found in a study of $(Ln_{0.5}M_{0.5})MnO_3$ phases by Damay et al.[11] Linear fits to three series with different $\langle r_A \rangle$ values were reported giving the parameters shown in Table 2. These parameters are comparable to the values obtained for the $x = 0.3$ series just mentioned and again show that p_1 decreases with increasing $\langle r_A \rangle$, although T_m^0 was not found to change significantly between series. The low-temperature magnetic phases (weak ferromagnetic, ferromagnetic, and two types of charge ordering) were found to lie within distinct regions in the $\langle r_A \rangle - \sigma^2$ plane.

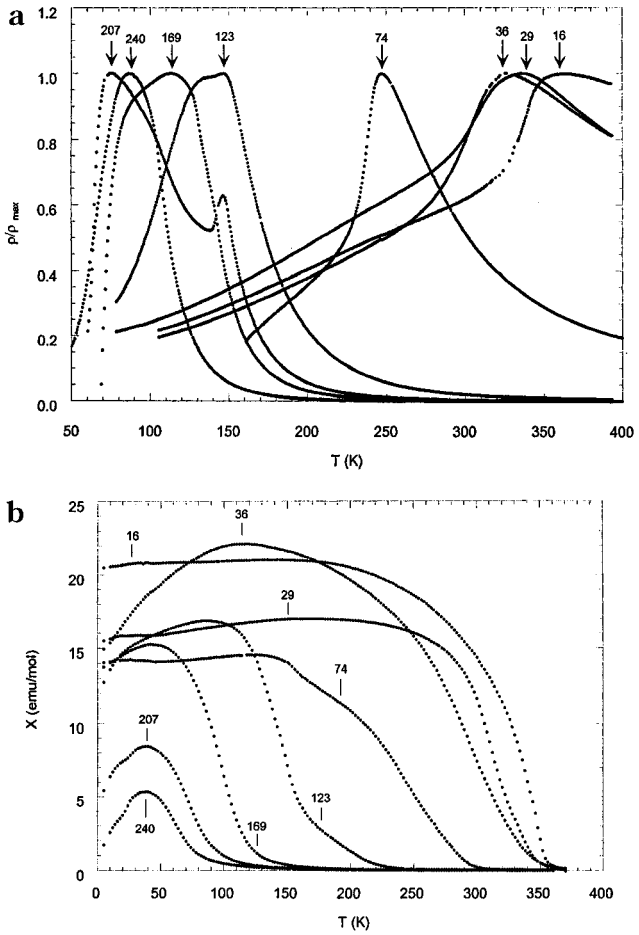

Figure 3. Plots of (a) normalized resistivity, and (b) magnetization/field ($H = 50$ mT) for the $(Ln_{0.7}M_{0.3})MnO_3$ perovskites listed in Table 1, with σ^2 ($\times 10^4$ Å^2) values labeled.

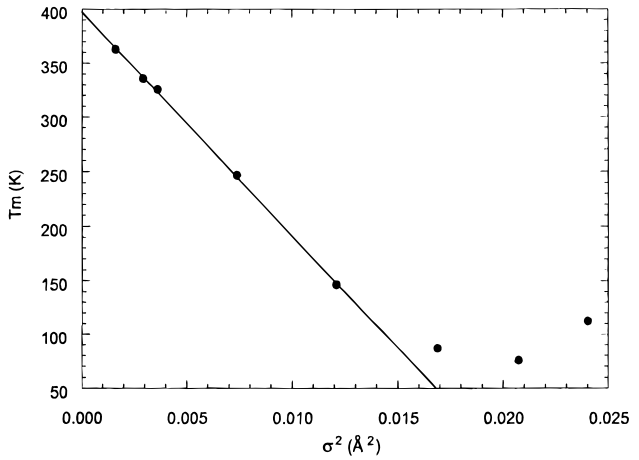

Figure 4. Variation of metal−insulator transition temperature T_m with A cation size variance σ^2 for the $(Ln_{0.7}M_{0.3})MnO_3$ perovskites in Table 1, showing a linear fit to data with $\sigma^2 < 0.015$ Å^2.

(ii) A_2CuO_4 Superconductors. The dependence of the superconducting critical temperature on σ^2 has recently been investigated in series of $(Ln_{1-x}M_x)_2CuO_4$ superconductors with the optimum doping level $x = 0.075$.[12] Two series of homogeneous $[(La,Nd)_{0.925}(Ca,Sr,Ba)_{0.075}]_2CuO_4$ compositions were prepared with a different mean radius $\langle r_A \rangle$ for each series. T_c shows a linear decrease with σ^2 in both cases (Figure 6), and the fitted parameters from eq 5 are presented in Table 2. As before, p_1

Table 2. Reported Parameters for $(Ln_{1-x}M_x)MnO_3$ Perovskites and $(Ln_{1-x}M_x)_2CuO_4$ Superconductors

x	$\langle r_A \rangle$ (Å)	T_e^0 (K)[a]	p_1 (K Å^{-2})	ref
		$(Ln_{1-x}M_x)MnO_3$ perovskites		
0.3	1.230	400(5)	20 600(500)	9
0.3	1.260	466(10)	15 500(1000)	10
0.5	1.225	330(10)	29 000(2000)	11
0.5	1.231	327(10)	22 300(2000)	11
0.5	1.237	330(10)	19 000(1500)	11
		$(Ln_{1-x}M_x)_2CuO_4$ superconductors		
0.075	1.212	31.6[b]		12
0.075	1.223	35.8(2)	6 100(110)	12
0.075	1.232	40.6(4)	2 450(90)	12

[a] T_e^0 is the value of the electronic transition temperature (metal−insulator for the manganites, superconductor−metal for the cuprates) extrapolated to zero variance; see eq 5. [b] This series shows a nonlinear variation due to a systematic inhomogeneity; T_e^0 is taken to be T_c for the first sample, which has $\sigma^2 \approx 0$.

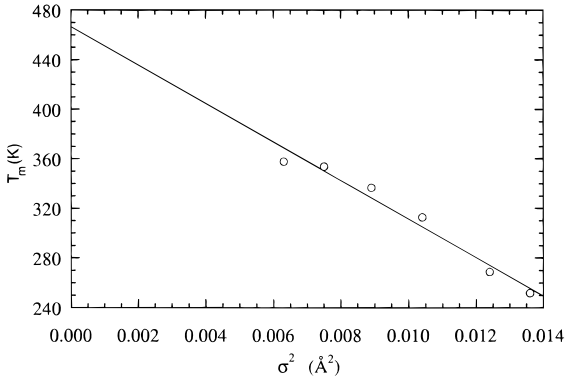

Figure 5. T_m versus σ^2 plot for a series of $(Ln_{0.7}M_{0.3})MnO_3$ perovskites with $\langle r_A \rangle = 1.26$ Å, with a linear fit shown.

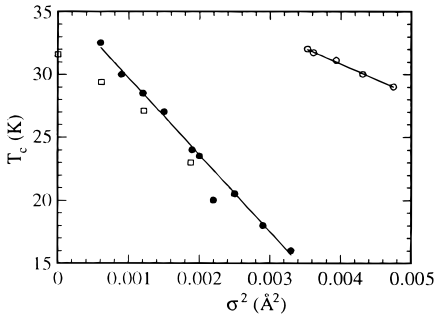

Figure 6. Variation of superconducting critical temperature T_c with A cation size variance σ^2 for series of $(Ln_{0.925}M_{0.075})_2CuO_4$ with fixed $\langle r_A \rangle = 1.212$ Å (open squares), 1.223 Å (filled circles), and 1.232 Å (open circles). Linear fits to the latter two series are shown.

decreases and T_e^0 ($=T_c^0$) increases with increasing $\langle r_A \rangle$.

Results for a third series of four samples with a smaller radius are also shown in Figure 6. The desired low σ^2 values required Ca contents decreasing steadily from 7.5% in the first composition to 5.3% in the fourth. The samples were annealed under a high oxygen pressure which is known to improve homogeneity for Ca-rich compositions,[13] but traces of $La_2CaCu_2O_6$ are evident in the powder X-ray diffraction pattern of the first sample and T_c shows a systematic but nonlinear decrease with σ^2. This result demonstrates that care has to be taken to avoid chemical inhomogeneities that vary systematically with σ^2, and hence mask the underlying trend in T_c.

3.2. Correlations between Mean Cation Size and Electronic Transition Temperatures. Variations of

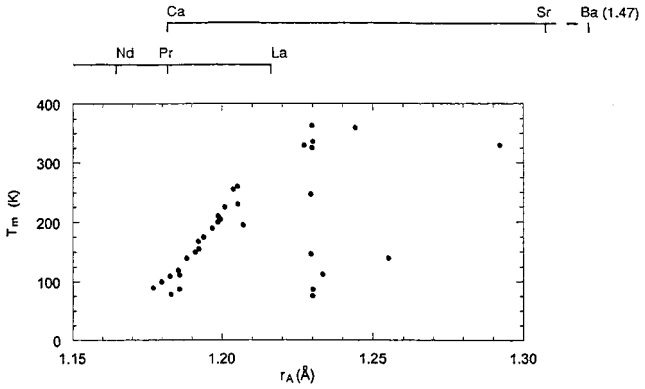

Figure 7. Plots of T_m values against average A cation radius $\langle r_A \rangle$ for reported $Ln_{0.7}M_{0.3}MnO_3$ compositions.[9] Ionic radii for individual cations are shown.

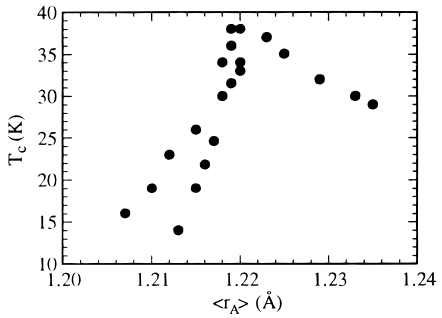

Figure 8. Plot of T_c for reported $(Ln_{0.925}M_{0.075})_2CuO_4$ materials[12] against average A cation radius $\langle r_A \rangle$.

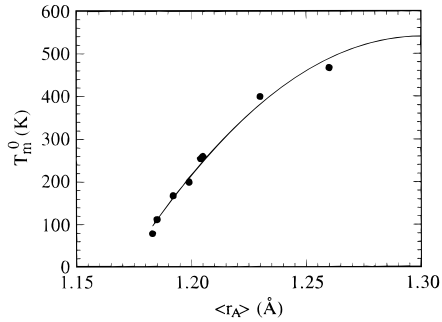

Figure 9. Plot of T_m^0 against $\langle r_A \rangle$ for reported $Ln_{0.7}M_{0.3}MnO_3$ perovskites showing the fit of eq 7.

electronic transition temperature T_e with mean A cation size $\langle r_A \rangle$ or tolerance factor have often been reported, although these have not taken the size variance effect into account. Figures 7 and 8, respectively, show the variations of T_m for $(Ln_{0.7}M_{0.3})MnO_3$ perovskites[9] and T_c for $(Ln_{0.925}M_{0.075})_2CuO_4$ superconductors[12] with $\langle r_A \rangle$.

To find the inherent dependence of T_e on $\langle r_A \rangle$, the size variance σ^2 has to be held constant. A special case is when $\sigma^2 = 0$, giving the disorder-corrected values of T_e^0. In the initial study of lattice effects on T_m in $(Ln_{0.7}M_{0.3})MnO_3$ perovskites,[9] p_1 was assumed to be constant over all radii $\langle r_A \rangle$ so that each T_m value in Figure 7 could be extrapolated back to T_m^0 using eq 5 by calculating σ^2 for the A site composition used. However, the results in Table 2 show that this assumption was very poor. To show the approximate $\langle r_A \rangle$ variation of T_m^0 (Figure 9), the extrapolated values from the two $(Ln_{0.7}M_{0.3})MnO_3$ series in Table 2 are shown together with reported T_ms for six samples with very little disorder ($\sigma^2 < 0.0005$ Å^2). These series are $(La_{0.7-y}Pr_yCa_{0.3})MnO_3$ ($y = 0$, 0.175, 0.35, 0.525, 0.6)[14] and $(La_{0.69}Y_{0.01}Ca_{0.3})MnO_3$.[15]

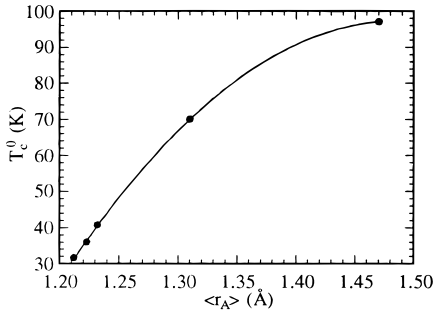

Figure 10. Plot of T_c^0 against $\langle r_A \rangle$ for optimally doped single-CuO_2-layer superconductors, with a fit of eq 7.

These series show a smooth increase with $\langle r_A \rangle$ that can be described by a quadratic function as discussed in the next section.

The disorder-corrected T_c^0 values for $(Ln_{0.925}M_{0.075})_2CuO_4$ superconductors also increase with $\langle r_A \rangle$,[12] although the range is too small to reveal the overall $\langle r_A \rangle$ dependence. However, by assuming that A cation effects predominate over other structural influences in determining T_c, then T_c^0 values can be obtained from other families of optimally doped superconductors that contain single CuO_2 layers such as the A_2CuO_4 materials, but have higher values of $\langle r_A \rangle$. In practice, this determination is very difficult because the compositions of other more complex cuprate superconductors cannot be controlled exactly. However, in the special case when the A sites are occupied by only one type of large cation (Sr or Ba), then the maximum observed T_c from the known single CuO_2 layer materials may be taken as the approximate T_c^0 for that A cation radius. The highest reported T_c for a single-layer material containing only Sr^{2+} ($r_A = 1.31$ Å) at the A sites is 70 K, reported for $(Tl,Pb)_{0.5}C_{0.5}Sr_2CuO_5$.[16] $Tl_2Ba_2CuO_{6+\delta}$ ($T_c = 93$ K)[17] and $HgBa_2CuO_{4+\delta}$ ($T_c = 97$ K)[18] both have only the large Ba^{2+} ($r_A = 1.47$ Å) cations in the A sites adjacent to the CuO_2 layers, and the latter provides an estimate of T_c^0 at this radius. Plotting these T_c^0 values with those from the three $(Ln_{0.925}M_{0.075})_2CuO_4$ series shows that the critical temperatures of optimally doped, disorder-free, single-layer cuprate superconductors also increase quadratically with $\langle r_A \rangle$ (Figure 10).

The variations of T_e shown in Figures 7 and 8 are rather similar and can be explained on the basis that T_e increases quadratically with mean size $\langle r_A \rangle$ but also decreases with increasing size variance σ^2. The ionic radii[5] of typical A site cations are 1.216−1.132 Å for Ln^{3+} = La − Sm and 1.18, 1.31, and 1.47 Å for M^{2+} = Ca, Sr, and Ba, respectively, as shown in Figure 7. Low $\langle r_A \rangle$ values are usually achieved with mixtures of Ln^{3+} and Ca^{2+}, which have comparable radii, so that the suppression of T_e due to size disorder is small and the inherent quadratic increase in T_e ($\approx T_e^0$) with $\langle r_A \rangle$ is apparent up to a maximum just above $r(La^{3+})$, which is usually close to the (La,Sr) composition. Larger $\langle r_A \rangle$ values require increasing substitution of Ca^{2+}/Sr^{2+} by Ba^{2+}, which is very much larger than the Ln^{3+} cations, so that an increasing size variance (σ^2) tends to reduce T_e and the increase in $\langle r_A \rangle$ tends to increase it. Hence, T_e is approximately constant at large $\langle r_A \rangle$ because of these opposing effects.

Superconductivity is also observed in doped bismuth oxide perovskites, and the difference between the critical temperatures of $(Ba,K)BiO_3$ ($T_c = 30$ K) and the recently reported $(Sr,K)BiO_3$ ($T_c = 12$ K)[19] is also consistent with the smaller $\langle r_A \rangle$ and larger σ^2 of the latter material ($r_A(K^+) = 1.55$ Å).

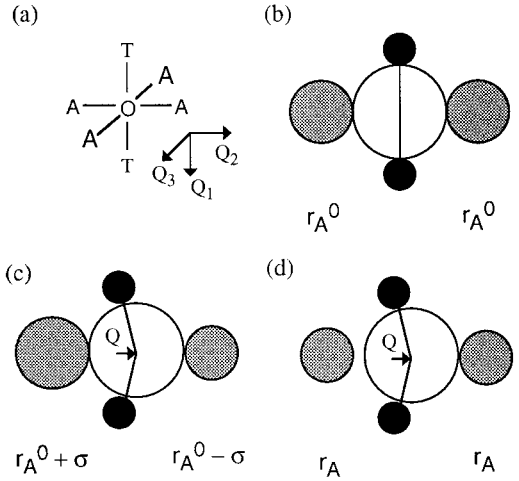

Figure 11. Hard sphere model for local oxygen displacements in ATO_3 perovskites. The ideal oxygen environment with A cations of radii r_A^0 is shown schematically in (a) (with displacement directions defined) and as spherical ions in (b) with only one of the two pairs of A cations displayed for clarity. Cation size disorder in (c) gives rise to an oxygen displacement $Q = \sigma$, and a reduction in the A site radius in (d) leads to the displacement $Q = r_A^0 - r_A$.

3.3. A Simple Model for Lattice Effects. The experimental results just presented indicate that the metal−insulator transition temperature in manganite perovskites and the superconducting critical temperature of single-layer cuprates both show a linear dependence on A cation size disorder σ^2 at constant radius $\langle r_A \rangle$ and a quadratic $\langle r_A \rangle$ dependence at constant σ^2 (=0). These two variations can be reconciled using a simple phenomenological model in which the changes in T_m or T_c are attributed to oxygen atom displacements. An ideal cubic ATO_3 perovskite structure has A cation radius r_A^0, defined as giving a tolerance factor $t = 1$ in eq 1. Each oxygen atom is coordinated octahedrally by two T cations and four A cations, with a linear T−O−T bridge (Figure 11a and b). Size mismatch due to one pair of A cations is represented by the large (radius $r_A^0 + v$) and small (radius $r_A^0 - v$) cations (Figure 11c). For this distribution, $v = \sigma$ ($\sigma = \sqrt{\sigma^2}$ is the standard deviation in the A cation size distribution) and the displacement of the oxygen atom in a hard sphere model is thus $Q = \sigma$. If the two A cations have the same size $r_A = r_A^0 - v$ (Figure 11d), then analogous oxygen displacements of magnitude $Q = v = r_A^0 - r_A$ occur because of the reduction in average size.

Experimentally, at constant $\langle r_A \rangle$, the electronic transition temperatures T_e have been found to vary as shown in eq 5, so, by analogy, at constant σ^2, the model just presented suggests that the size dependence should be

$$T_e = T_e^* - p_2(r_A^0 - \langle r_A \rangle)^2 \qquad (6)$$

where T_e^* is the transition temperature extrapolated to $\langle r_A \rangle = r_A^0$, and the coefficient p_2 is analogous to p_1. This function has been used to fit the T_m^0 and T_c^0 data in Figures 9 and 10. The same T_m^0 data from Figure 9 are plotted against $(r_A^0 - \langle r_A \rangle)^2$ in Figure 12, demon-

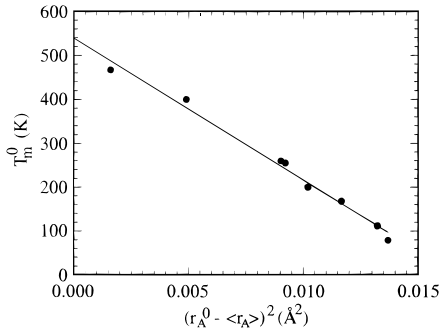

Figure 12. Plot of disorder corrected $T_m{}^0$ for $Ln_{0.7}M_{0.3}MnO_3$ perovskites from Figure 9 against $(r_A{}^0 - \langle r_A \rangle)^2$, showing the linear fit of eq 7.

strating the linear correlation. Here, $r_A{}^0 = 1.30$ Å from the perovskite tolerance factor relation, and the fitted parameters are $T_m{}^* = 540(15)$ K and $p_2 = 32\ 300(1500)$ K. In this case, $T_m{}^*$ is an estimate of the maximum metal-insulator transition temperature $T_m{}^m$ for an ideal $(Ln_{0.7}M_{0.3})MnO_3$ perovskite in which all the cations have the ideal radius $r_A{}^0$. The coefficient p_2 is of comparable magnitude to the p_1 values for manganites in Table 2, supporting the analogy between mean size and size mismatch in this simple model. It is also notable that the minimum $\langle r_A \rangle$ value at which the ferromagnetic metallic state is observed in $(Ln_{0.7}M_{0.3})MnO_3$ perovskites corresponds to $(r_A{}^0 - \langle r_A \rangle)^2 \approx 0.014$ Å^2, which essentially coincides with the upper value of σ^2 (0.015 Å^2) at which homogeneous samples were found in the reported study[9] (compare Figures 4 and 12). This similarity suggests a close analogy between the mean size and size disparity effects on the stability limit of the ferromagnetic conducting phase.

3.4. Effects of Cation Size Variance on Other Physical Properties. The studies just presented have concentrated on establishing links between electronic transition temperatures and A cation size or disorder, but some relationships between the latter quantities and the physical properties of interest have also been observed.

The ferromagnetic metal-to-paramagnetic insulator transition in $(Ln_{1-x}M_x)MnO_3$ perovskites is associated with large negative magnetoresistances, quantified by the ratio of resistivities in zero and applied fields, $\rho(0)/\rho(B)$, which has a maximum value R_B at a temperature close to T_m. The magnitude of R_B increases greatly as T_m is shifted to lower temperatures, from values of 1−2 at room temperature up to R_{5T} values of $\sim 10^5$ at temperatures of ~100 K,[20] and so is increased by increasing σ^2 or decreasing $\langle r_A \rangle$ as these both reduce T_m according to eqs 5 and 6. It was noted[9] that reported data for $(Ln_{0.7}M_{0.3})MnO_3$ phases having similar T_ms show that R_B is suppressed by increasing A site disorder σ^2. For example, $Pr_{0.7}Sr_{0.05}Ca_{0.25}MnO_3$ ($\sigma^2 = 0.0008$ Å^2) has $R_{5T} = 250\ 000$ at 85 K,[20] whereas $La_{0.6}Y_{0.1}Ca_{0.3}MnO_3$ ($\sigma^2 = 0.0022$ Å^2) has $R_{5T} = 40$ at 120 K.[15] Similarly, $La_{0.525}Pr_{0.175}Ca_{0.3}MnO_3$ ($\sigma^2 = 0.0003$ Å^2) has $R_{5T} = 10$ at 210 K,[14] whereas $Nd_{0.7}Sr_{0.3}MnO_3$ ($\sigma^2 = 0.0044$ Å^2) has $R_{6T} = 1.5$ at 195 K.[21]

The exact size matching of Pr^{3+} and Ca^{2+} (both with $r = 1.18$ Å) results in negligible size variance ($\sigma^2 < 10^{-6}$ Å^2) throughout the $Pr_{1-x}Ca_xMnO_3$ system, which enables a variety of charge- and spin-ordered states to be observed.[22] These phases are nonmetallic because of the small $\langle r_A \rangle$, although a transition to the ferromagnetic metallic state in $Pr_{0.7}Ca_{0.3}MnO_3$ can be induced by applied pressure,[23] magnetic fields (resulting in very large magnetoresistances),[22,23] or chemical substitutions with La or Sr.[14,19] Sundaresan et al. have shown that in the latter case, increasing the A site size disorder is sufficient to induce the ferromagnetic conducting state.[24] A study of $Ln_{0.5}M_{0.5}MnO_3$ perovskites also shows that charge-ordering transitions are sensitive to σ^2.[11]

In the study by alternating current (ac) susceptometry[12] of powdered $(Ln_{0.925}M_{0.075})_2CuO_4$ samples with fixed $\langle r_A \rangle = 1.223$ Å, it was found that both T_c (Figure 6) and the diamagnetic volume fraction fell with increasing A site disorder, from 20% of perfect diamagnetism at $\sigma^2 = 0.0006$ Å^2 to zero at $\sigma^2 = 0.0035$ Å. Furthermore, for samples with σ^2 above this limit, no superconducting transition was observed. This result suggests that the penetration depth for superconductivity decreases systematically with increasing σ^2.

3.5. Structural Effects of Cation Size Variance. The only study carried out so far on a series of materials with constant doping level and mean A cation size $\langle r_A \rangle$ but variable σ^2 has been performed on four of the samples listed in Table 1, which show a linear decrease of T_m with σ^2.[25,26] These samples have been studied by time-of-flight powder neutron diffraction at 4 K to minimize thermal effects. The crystal structures were Rietveld-refined from data covering a wide *d* spacing range, enabling the atomic displacement factors ('temperature factors') to be refined accurately. Some of the results of the refinements are shown in Table 3 and Figure 13. These structures have the $GdFeO_3$-type orthorhombic superstructure of the ideal cubic perovskite lattice. Small changes in the cell parameters and mean Mn−O distances and Mn−O−Mn angles with σ^2 are evidenced, but much larger changes in disordered local structure also occur as described later. The refined Mn magnetic moments are close to the ideal value of 3.7 μ_B and show no significant variation with σ^2, which rules out an increasing spin disorder as the cause of the decrease of T_m across the series.

This study enables the disordered displacements of the oxygen atoms around their mean positions to be compared with those predicted by the simple model in Figure 11. In the orthorhombic superstructure adopted by these four perovskites there are two crystallographically distinct oxygen atoms. Anisotropic refinement of their atomic displacement factors gave the principal mean squared displacements u_i in the three perpendicular directions defined in Figure 11a. The u_i values contain contributions from thermal vibrations (phonons) and static disorder of the atoms around their mean positions, which are generally not additive quantities. However, the approximately linear increases in the u_i components with σ^2 in Figure 13 show that at 4 K the increase in u_i is due mainly to increasing static disorder resulting from the size mismatch at the neighboring A cation sites. The change $\Delta u_i = u_i(\sigma^2) - u_i(\sigma^2 = 0)$ is thus an experimental measure of the mean-squared displacements due to cation size disparity $\langle Q_i{}^2 \rangle$, as shown in Figure 11.

The simple model in Figure 11 shows that in an ideal cubic perovskite with mean A cation radius $r_A{}^0$, cation

Table 3. A Site Compositions with σ^2 Values and Parameters from 4 K Powder Neutron Refinements for $AMnO_3$ Perovskites[a]

A site composition	σ^2 (Å^2)	a (Å)	b (Å)	c (Å)	V (Å^3)	μ_{Mn} (μB)	mean Mn−O (Å)	mean Mn−O−Mn (deg)
$La_{0.70}Ca_{0.11}Sr_{0.19}$	0.0016	5.4586(1)	7.7146(2)	5.5005(1)	231.63(1)	3.55(1)	1.954	163.3
$La_{0.32}Pr_{0.38}Sr_{0.30}$	0.0029	5.4544(1)	7.7067(2)	5.4953(1)	231.00(1)	3.61(1)	1.954	162.7
$Pr_{0.70}Sr_{0.23}Ba_{0.07}$	0.0074	5.4602(2)	7.7102(2)	5.4852(2)	230.92(2)	3.55(1)	1.957	161.3
$Nd_{0.70}Sr_{0.16}Ba_{0.14}$	0.0123	5.4680(2)	7.7263(3)	5.4800(2)	231.52(1)	3.56(1)	1.961	160.7

[a] See also Table 1.

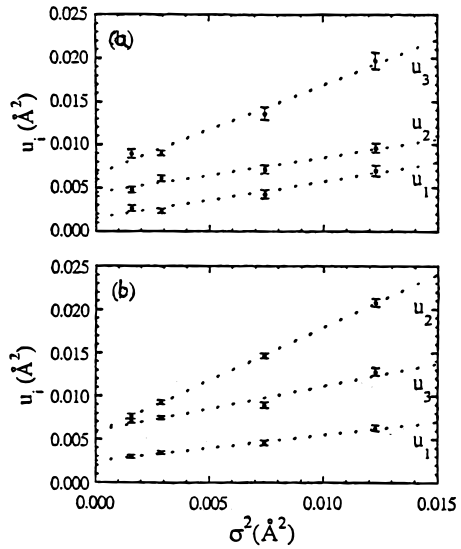

Figure 13. Variation of the principal mean squared oxygen displacements in the directions shown in Figure 11a for the 4 K orthorhombic $Ln_{0.7}M_{0.3}MnO_3$ structures (Table 1) with A site disorder at (a) the O(1) site (0.49, 1/4, 0.05), and (b) the O(2) site (0.27, 0.03, −0.27).

Table 4. Rates of Increase in the Three Principal Mean Squared Oxygen Displacements with A Cation Size Variance at 4 K for the Two Oxygen Sites in the Orthorhombic $(Ln_{0.7}M_{0.3})MnO_3$ Series[a]

site	$\Delta u_1/\sigma^2$	$\Delta u_2/\sigma^2$	$\Delta u_3/\sigma^2$	$\langle\Delta u\rangle/\sigma^2$
O(1) (×4)	0.30	0.52	1.23	0.68
O(2) (×8)	0.43	0.41	1.04	0.63
mean	0.39	0.45	1.10	0.65
predicted[b]	0	1	1	0.67

[a] With $\langle r_A\rangle = 1.23$ Å (Figure 13). [b] For $\langle r_A\rangle = r_A^0$ from the simple model shown in Figure 11.

mismatch only gives rise to oxygen displacements perpendicular to the Mn−O−Mn axis; that is, $Q_1^2 = 0$ and $Q_2^2 = Q_3^2 = \sigma^2$, giving a mean value $\langle Q^2\rangle/\sigma^2 = 0.67$. These results are compared with the experimental Δu_i values in Table 4. It is notable that the mean $\Delta u_i/\sigma^2$ values for the two oxygen sites and the overall mean of 0.65 are in excellent agreement with the predicted $\langle Q^2\rangle/\sigma^2 = 0.67$ increase in mean squared oxygen displacement with A site disorder. This result verifies the use of σ^2 as a functional for the total displacive disorder of the oxygen atoms due to A site cation size disorder in perovskites. However, the individual $\Delta u_i/\sigma^2$ values are rather different from the predicted values because the structures deviate significantly from the ideal cubic perovskite arrangement. These values are orthorhombic with $\langle r_A\rangle = 1.23$ Å significantly below $r_A^0 = 1.30$ Å so that the environment around oxygen is less symmetric than in Figure 11 due to bending of the T−O−T angle to ∼160°. In particular, the displacements due to disorder parallel to the T...T direction, u_1, increase significantly with σ^2, and this result provides an explanation for the increase in the coefficient p_1 with decreasing $\langle r_A\rangle$ (see Table 2). If as discussed later these displacements are primarily responsible for the decrease in T_m with increasing σ^2, then the observation that they are more easily induced with decreasing $\langle r_A\rangle$ as the structure becomes more distorted accounts for the trend in p_1.

4. Discussion

4.1. Variables Controlling Lattice Effects. From the studies just presented it is clear that the electronic properties of ATO_3 perovskites and related materials are controlled by three factors. These factors are the average charge of the A site cations, which determines the electron concentration (oxidation state) of the transition metal, the mean A cation radius $\langle r_A\rangle$, and the distribution of A cation radii, which can be conveniently parametrized by the variance σ^2. The use of σ^2 assumes that the A cation distribution is random, which is not strictly true because neighboring cations interact with each other through their strain fields, and local cation ordering or microphase separation may result. Nevertheless, the experimental studies to date indicate that σ^2 is a sufficient description of the cation size mismatch for most purposes and it has the advantage of being a standard statistical quantity that is defined for any distribution through eq 2. Care has to be taken to ensure that samples are homogeneous and oxygen stoichiometric and in particular to avoid any chemical inhomogenities that vary systematically with σ^2. It is also preferable to avoid any systematic dependence of σ^2 on individual ionic radii, which are only experimental 'best estimates',[5] by varying the A cations used where possible (e.g., as in Table 1).

An overall electronic phase diagram for a given perovskite system such as $AMnO_3$ requires three dimensions for the aforementioned chemical variables plus further dimensions for physical variables (temperature, pressure, magnetic field strength, etc.). Even to determine the four-dimensional $T(x, \langle r_A\rangle, \sigma^2)$ phase diagram will require very many samples. Conventional phase diagrams such as the $T-x$ plane for a given $(Ln_{1-x}M_x)MnO_3$ system provide chemically convenient but physically arbitrary sections through this space. It is important to recognize that at a given doping level, all chemically possible samples lie within a restricted $\langle r_A\rangle - \sigma^2$ region as shown schematically for $(Ln_{0.7}M_{0.3})MnO_3$ in Figure 14. This region does not usually include the ideal disorder-free perovskite ($\sigma^2 = 0$, $\langle r_A\rangle = r_A^0$), although an experimental estimate of the properties of this and other hypothetical structures can be obtained by extrapolation from known phases within the accessible $\langle r_A\rangle - \sigma^2$ region.

Figure 14 also illustrates some of the experimental difficulties in preparing series of samples with fixed $\langle r_A\rangle$

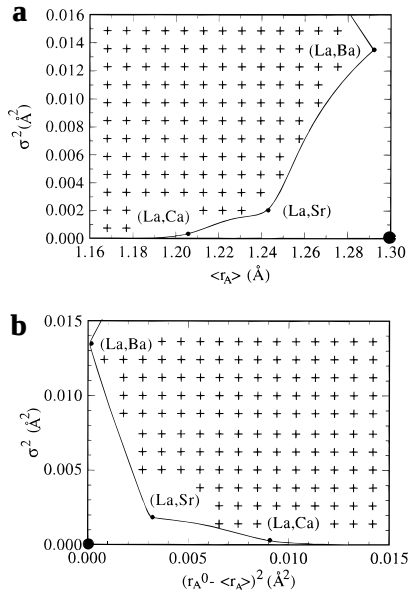

Figure 14. (a) The $\langle r_A \rangle - \sigma^2$ field, also shown on a σ^2 versus $(r_A{}^0 - \langle r_A \rangle)^2$ plot in (b), for $Ln_{0.7}M_{0.3}MnO_3$ perovskites. The decorated region contains chemically possible compositions with the simple (La,M) combinations marked. The large point corresponds to the hypothetical, cubic disorder free perovskite.

and variable σ^2. At large $\langle r_A \rangle$, approaching the maximum possible value that is always for the (La,Ba) composition, the range of σ^2 is very small with a minimum $\sigma^2 \gg 0$, so the correlation of physical properties with σ^2 is difficult to establish and extrapolations to $\sigma^2 = 0$ are subject to large errors. The $(Ln_{0.7}M_{0.3})MnO_3$, $\langle r_A \rangle = 1.26$ Å series (Figure 5) and $(Ln_{0.925}M_{0.075})_2CuO_4$, $\langle r_A \rangle = 1.232$ Å series (Figure 6), both of which start at the smallest possible σ^2 value, illustrate this problem. With medium values of $\langle r_A \rangle$, close to the (La,Sr) composition, samples with a wide range of σ^2 and T_e values can be prepared. At small $\langle r_A \rangle$, a very wide range of σ^2 is possible, but the perovskite structure is already destabilized by the small $\langle r_A \rangle$, which may lead to inhomogeneity when disorder is introduced. Also the maximum transition temperature $T_e{}^0$ is considerably reduced at small $\langle r_A \rangle$, leaving a narrow T_e range to be studied with increasing disorder.

Despite the problems just mentioned, results to date (Table 2) are generally consistent and show that electronic transition temperatures decrease linearly with σ^2 and the negative slope p_1 increases as $\langle r_A \rangle$ decreases. Extrapolation to zero size variance yields an estimate of the disorder-free value $T_e{}^0$, which increases with $\langle r_A \rangle$ up to the maximum $r_A{}^0$ value for a simple ATO_3 perovskite. The analogous dependence of T_e on $\langle r_A \rangle$ at constant σ^2 has not yet been thoroughly investigated, and will again be limited by the shape of the $\langle r_A \rangle - \sigma^2$ space already discussed. However, the analogy described previously leads to a quadratic function (eq 6) which is supported by data for the special case of $T_e{}^0$ versus $\langle r_A \rangle$ in two cases (Figures 9 and 10).

Combining eqs 5 and 6 gives a general expression for lattice effects on an electronic transition at a constant doping level, where $T_e{}^m$ is the maximum transition temperature for the ideal, disorder-free cubic composition

$$T_e = T_e{}^m - p_1(\langle r_A \rangle)\sigma^2 - p_2(\sigma^2)(r_A{}^0 - \langle r_A \rangle)^2 \qquad (7)$$

The dependences of p_1 and p_2 on $\langle r_A \rangle$ and σ^2, respectively, are not yet known. From this equation, it can be seen that in a given $(Ln_{1-x}M_x)TO_3$ system (Figure 2) in which the doping level ($n = x$) is also varying, changes in all of these quantities contribute to the observed T_e variation.

4.2. The Origin of the Lattice Effects. Mean A cation size and size disparity are not necessarily equivalent; for example, they affect the magnetoresistance properties of $AMnO_3$ perovskites differently, but the results just reviewed show that they both suppress the metal−insulator transition temperature in $AMnO_3$ perovskites and the critical temperature in A_2CuO_4 in similar ways. To a good approximation, these electronic transition temperatures decrease quadratically with lattice displacements of the oxygen atoms due to A cation mismatch or to a reduction in the mean A cation radius from the ideal value. The observation of this effect in both classes of material show that it is not specific to the physics of double exchange or the superconducting mechanism, but is a more general phenomenon. Two types of explanation can be advanced, either the strength of the electronic interaction is reduced by the lattice displacements or there is a lattice strain contribution to the transition energy in addition to the electronic term.

The first of these types of explanation has been widely used to account for A cation size (tolerance factor) effects on transition temperatures in perovskites. The strength of the electronic interaction is characterized by a hopping energy, transfer integral, bandwidth, or some other energy parameter. This depends on the mutual overlap of transition metal d orbitals with oxygen p orbitals and so is reduced by changes in T−O bond lengths and in particular T−O−T angles. This approach is qualitatively successful because decreases in T_e within series of related compositions are generally found to correlate with increased bending of the T−O−T bridges. A more sophisticated treatment also involving changes in the T−O distances has been reported for the $(Ln_{0.7}M_{0.3})MnO_3$ perovskites, giving a good correlation with T_m,[27] although small changes in bandwidth (~3%) are required to explain a large decreases of T_m from 350 to 100 K.

However, it is difficult to account for the close analogy between the effects of cation size and disorder on T_e in an electronic picture. In the usual band description of metal−insulator transitions,[28] increasing $(r_A{}^0 - \langle r_A \rangle)^2$ results in a Mott−Hubbard-type transition through the *reduction* of the bandwidth to below the Hubbard U energy. However, increasing disorder through σ^2 leads to an *increase* in bandwidth but with an increasing proportion of localized states at the extremities of the band above the upper and below the lower of the two mobility edges. An Anderson-type metal-to-insulator transition occurs when one of the mobility edges crosses the Fermi level as disorder increases. Why these transitions should both lead to analogous quadratic dependences with lattice displacement and whether any rationale can be extended to the superconducting transition in copper oxides is not clear in an electronic picture.

The alternative type of explanation for the observed lattice effects involves their associated strain energies by assuming that a small structural distortion occurs at T_e in transition-metal perovskites. Both metal−

insulator and superconductor−metal transitions redistribute the energies and momenta of electrons in bands of d-orbital character. These influence the T−O bonding, in particular when the Fermi level lies within a band derived from the strongly σ-antibonding T:e_g orbitals, as is the case in both the manganite perovskites and the cuprate superconductors.

At a given doping level, the maximum electronic transition temperature T_e^m occurs for the ideal undistorted perovskite structure with all A cations having radius r_A^0. Writing $T_e^m = \Delta H_e^m/\Delta S_e^m$ where ΔH_e^m and ΔS_e^m are respectively the transition enthalpy and entropy,[29] then if a small structural distortion occurs at the transition, ΔH_e^m may be written as

$$\Delta H_e^m = \Delta H_e^{m\prime} + (NK/2)\langle Q_m^2\rangle \quad (8)$$

where the strain term contains the number N (=6) of T−O bonds per T atom, $\langle Q_m^2\rangle$ is the mean squared oxygen displacement occurring at the transition, K is the mean T−O force constant for the distortion, and $\Delta H_e^{m\prime}$ contains the electronic and any other lattice (e.g., phonon) contributions.

If additional oxygen displacements Q_d in the same direction as Q_m (or having the same irreproducible representation when considering symmetry-coupled displacements) are introduced by some A cations having nonideal radii ($r_A \neq r_A^0$), then the transition enthalpy becomes

$$\Delta H_e = \Delta H_e^{m\prime} + (NK/2)(\langle Q_m^2\rangle - \langle Q_d^2\rangle)$$

$$= \Delta H_e^m - (NK/2)\langle Q_d^2\rangle \quad (9)$$

Hence,

$$T_e = T_e^m - (NK/2\Delta S_e^m)\langle Q_d^2\rangle \quad (10)$$

assuming that $\Delta H_e^{m\prime}$ and ΔS_e^m are relatively insensitive to the additional oxygen displacements. Following the simple hard sphere description in Section 3.3 and Figure 11, each local oxygen displacement due to one of the pair of neighboring A cations has the magnitude $Q_d \leq (r_A^0 - r_A)$. This result enables $\langle Q_d^2\rangle$ to be expanded:

$$\langle Q_d^2\rangle = C\langle (r_A^0 - r_A)^2\rangle$$

$$= C\{[\langle (r_A^0 - r_A)^2\rangle - \langle r_A^0 - r_A\rangle^2] + \langle r_A^0 - r_A\rangle^2\} \quad (11)$$

$$= C[\sigma^2 + (r_A^0 - \langle r_A\rangle)^2] \quad (12)$$

where C is a constant in the range $0 < C < 2$ (the upper value of 2 arises from the two pairs of A cations in perpendicular planes; see Figure 1). Thus, from eq 10, eq 13 can be written

$$T_e = T_e^m - (CNK/2\Delta S_e^m)[\sigma^2 + (r_A^0 - \langle r_A\rangle)^2] \quad (13)$$

This relationship accounts for the form of eq 7. Equation 11 separates $\langle Q_d^2\rangle$ into incoherent and coherent terms showing that the σ^2 and $(r_A^0 - \langle r_A\rangle)^2$ dependences of T_e are respectively due to incoherent and coherent strain contributions to the overall transition enthalpy. The strain coefficients p_1 and p_2 both have magnitude $CNK/2\Delta S_e^m$ in this simplest approximation. The parameter C is a measure of how efficiently the A cations produce oxygen displacements Q_d with the same symmetry as the distortion occurring at the electronic transition. It is not easily estimated from first principles, but a variation of C with $\langle r_A\rangle$ can account for the $\langle r_A\rangle$ dependence of p_1 in Table 1.

For the $(Ln_{1-x}M_x)MnO_3$ perovskites there is clear evidence for a structural discontinuity at the metal−insulator transition. In particular, a pronounced discontinuity in u_1, the mean squared oxygen displacement parallel to the Mn−O bonds in Figure 13 is observed.[26,30] This displacement, unlike the perpendicular components u_2 and u_3, moves the oxygen atom closer to one neighboring Mn than another, as is found in the cooperatively Jahn−Teller distorted parent compound $LaMnO_3$.[31] The changes in $(Ln_{1-x}M_x)MnO_3$ at T_m are consistent with a change from dynamic Jahn−Teller distortions below T_m to static distortions above the transition, as predicted by polaronic models for electronic transport.[32,33] The static distortions are large but are usually not long-range ordered because of the dilution of Jahn−Teller active Mn^{3+} with inactive Mn^{4+}.

The correlation between A cation size disorder and T_m can be demonstrated through eq 13 for the $(Ln_{0.7}M_{0.3})MnO_3$ series in Table 1. Figures 4 and 13 show that T_m decreases linearly and u_1 increases linearly with σ^2. We can then estimate $p_1 \approx CNK/\Delta S_m$. There are $N = 6$ Mn−O bonds per Mn cation. An experimental upper limit of $C = 0.4$ derives from Figure 13 because this is the observed value of $\Delta u_1/\sigma^2$, although the Jahn−Teller active proportion of the observed u_1 squared-displacements is unknown. The parameter ΔS_m is approximated by the dominant magnetic entropy change, $\Delta S_m \approx k_B \ln(2\langle S\rangle + 1) \approx 1.5k_B$ for $\langle S\rangle = 1.85$ and the mean Mn−O force constant is estimated to be $K \approx 100$ Nm^{-1}.[34] These results give $p_1 \approx 60\,000$ K Å^{-2}, which is comparable to the observed $p_1 = 20600$ K Å^{-2} given the approximate magnitudes of the various quantities and the unknown proportion of Jahn−Teller active displacements due to A cation size variance.

Whether a structural change occurs at the critical transition in copper oxides superconductors is still uncertain, but evidence for a very slight anomaly has been found in some materials [e.g., in a recent neutron diffraction and extended X-ray absorption fine structure (EXAFS) study of $HgBa_2CuO_{4+\delta}$].[35] The excess entropy below the transition is only ~0.05 k_B per Cu atom, and so even a very slight structural change could still give rise to the relatively large lattice sensitivity of T_c observed in Figures 6 and 10 through eq 13. In the study of $(Ln_{0.925}M_{0.075})_2CuO_4$ superconductors with $\langle r_A\rangle = 1.223$ Å,[12] the purely structural orthorhombic−tetragonal change also varies with σ^2, with an average rate of change about six times that for T_c. These comparable magnitudes also support the general case for a similar strain-based origin for the lattice sensitivities of both the electronic and the structural transitions.

4.3. Application to Other Defects. Substitutional defects that have been used to control lattice disorder in all of this work are straightforward to parametrize through the size variance. Other point defects such as interstitials or vacancies can also be used to control the electronic properties of perovskite compounds. For example, cation vacancies can induce the ferromagnetic conducting state in $La_{1-x}Mn_{1-x}O_3$ ('$LaMnO_{3+\delta}$')[36] and

oxygen interstitials lead to superconductivity in $La_2CuO_{4+\delta}$.[37] In both cases, effects such as those in Figure 2 occur. The doping is easily found from chemical analysis but the average lattice effect, analogous to changing $\langle r_A \rangle$, and the disorder are more difficult to parametrize and study systematically. One approach may be to compare the observed T_es with the disorder-corrected T_e^0 values obtained from the cation substitution studies just mentioned.

5. Conclusions

The electronic properties of ATO_3 perovskites and related materials are complex and vary considerably from one transition metal to another. Despite this variability, the electronic transition temperatures appear to have a simple dependence on oxygen displacements due to changes in mean A cation size or size mismatch that are common to at least two different classes of material. The quadratic nature of these correlations and the magnitudes of the changes are consistent with a lattice strain contribution to the transition enthalpies. The use of the A cation size variance in addition to the mean A cation radius and the doping level provides a set of three functionals that can be used to classify the properties of all the perovskites for a given transition metal. This approach is recent and only a small number of studies have been performed so far. Further work is needed to extend this methodology to other perovskite systems and to test further the proposed quadratic relationships.

Acknowledgment. I am very grateful to my coworkers Andrei Kharlanov, Judith McAllister, and Lide Rodriguez for performing the experimental studies that have been reviewed in this paper, and to A. Maignan and B. Raveau for supplying preprints. I acknowledge EPSRC for the provision of neutron facilities at Rutherford Appleton Laboratory.

References

(1) Cox, P. A. *Transition Metal Oxides*; International Series of Monographs on Chemistry: 27; Oxford Science Publications: Oxford, 1992.
(2) Rao, C. N. R.; Raveau, B. *Transition Metal Oxides*; VCH: New York, 1995.
(3) Burns, G. *High-Temperature Superconductivity*; Academic: New York, 1992.
(4) Rao, C. N. R.; Cheetham, A. K. *Adv. Mater.* **1997**, *9*, 1009.
(5) Radii for 9-fold coordination in oxides have been taken from Shannon, R. D. *Acta Crystallogr.* **1976**, *A32*, 751.
(6) Geller, S. *J. Chem. Phys.* **1956**, *24*, 1236.
(7) Goodenough, J. B.; Zhou, J.-S. *Chem. Mater.* **1998**, *10*, 2980−2993. Rao, C. N. R.; Arulraj, A.; Santosh, P. N.; Cheetham, A. K. *Chem. Mater.* **1998**, *10*, 2714−2722. Raveau, B.; Maignan, A.; Martin, C.; Hervieu, M. *Chem. Mater.* **1998**, *10*, 2641−2652.
(8) Tokura, Y. et al. *J. Appl. Phys.* **1996**, *79*, 5288.
(9) Rodriguez-Martinez, L. M.; Attfield, J. P. *Phys. Rev. B* **1996**, *54*, R15622.
(10) Rodriguez-Martinez, L. M.; Attfield, J. P., unpublished results.
(11) Damay, F.; Martin, C.; Maignan, A.; Raveau, B. *J. Appl. Phys.* **1997**, *82*, 6181.
(12) Attfield, J. P.; Kharlanov, A. L.; McAllister, J. A. *Nature* **1998**, *394*, 157.
(13) Dabrowski, B. et al. *Physica C* **1993**, *217*, 455.
(14) Hwang, H. Y.; Cheong, S.-W.; Radaelli, P. G.; Marezio, M.; Batlogg, B. *Phys. Rev. Lett.* **1995**, *74*, 914.
(15) Maignan, A.; Simon, Ch.; Caignaert, V.; Raveau, B. *J. Appl. Phys.* **1996**, *79*, 7891.
(16) Huve, M.; Michel, C.; Maignan, A.; Hervieu, M.; Martin, C.; Raveau, B. *Physica C* **1993**, *205*, 219.
(17) Wagner, J. L.; Chmaissem, O.; Jorgensen, J. D.; Hinks, D. G.; Radaelli, P. G.; Hunter, B. A.; Jensen, W. R. *Physica C* **1997**, *277*, 170.
(18) Asab, A.; Armstrong, A. R.; Gameson, I.; Edwards, P. P. *Physica C* **1995**, *255*, 180.
(19) Kazakov, S. M.; Chaillout, C.; Bordet, P.; Capponi, J. J.; Nunez-Regueiro, M.; Rysak, A.; Tholence, J. L.; Radaelli, P. G.; Putilin, S. N.; Antipov, E. V. *Nature* **1997**, *390*, 148.
(20) Raveau, B.; Maignan, A.; Caignaert, V. *J. Solid State Chem.* **1995**, *117*, 424.
(21) Mahesh, R.; Mahendiran, R.; Raychaudhuri, A. K.; Rao, C. N. R. *J. Solid State Chem.* **1995**, *120*, 204.
(22) Tomioka, Y.; Asamitsu, A.; Kuwahara, H.; Moritomo, Y.; Tokura, Y. *Phys. Rev. B* **1996**, *53*, R1689.
(23) Hwang, H. Y.; Palstra, T. T. M.; Cheong, S.-W.; Batlogg, B. *Phys. Rev. B* **1995**, *52*, 15046.
(24) Sundaresan, A.; Maignan, A.; Raveau. B. *Phys. Rev. B* **1997**, *56*, 5092.
(25) Rodriguez-Martinez, L. M.; Attfield, J. P. *Mater. Sci. Forum* **1998**, *278*, 738.
(26) Rodriguez-Martinez, L. M.; Attfield, J. P. *Phys. Rev. B* **1998**, *58*, 2426.
(27) Radaelli, P. G. et al. *Phys. Rev. B* **1997**, *56*, 8265.
(28) Mott, N. F. *Metal−Insulator Transitions*; Taylor and Francis: London, 1990.
(29) ΔH_e^m and ΔS_e^m are non-zero only for a first order transition, whereas the superconducting transition and, in many cases, the metal−insulator transition, are second order. In these cases, $T_e^m \sim \Delta H_e^m(T)/\Delta S_e^m(T)$ where $\Delta H_e^m(T)$ and $\Delta S_e^m(T)$ are now the excess enthalpy and entropy of the low temperature phase for $T < T_e^m$. [The simplest analytical form of the excess free energy gives $T_e^m = 2\Delta H_e^m(0)/\Delta S_e^m(0)$.] The following arguments may still be used although a small numerical factor is introduced into the expressions for T_e.
(30) Radaelli, P. G.; Marezio, M.; Hwang, H. Y.; Cheong, S.-W.; Batlogg, B. *Phys. Rev. B* **1996**, *54*, 8992.
(31) Norby, P.; Krogh Andersen, I. G.; Krogh Andersen, E.; Andersen, N. H. *J. Solid State Chem.* **1995**, *119*, 191.
(32) Roder, H.; Zang, J.; Bishop, A. R. *Phys. Rev. Lett.* **1996**, *76*, 1356.
(33) Millis, A. J.; Littlewood, P. B.; Shraiman, B. I. *Phys. Rev. Lett.* **1995**, *74*, 5144.
(34) K has been estimated to be in the range 30−300 Nm^{-1} by Millis, A. J.; *Phys. Rev. B* **1996**, *53*, 8434.
(35) Bordet, P.; Duc, F.; Radaelli, P. G.; Lanzara, A.; Saini, N.; Bianconi, A.; Antipov, E. V. *Physica C* **1997**, *282*, 1081.
(36) Arulraj, A.; Mahesh, R.; Subbanna, G. N.; Mahendiran, R.; Raychaudhuri, A. K.; Rao, C. N. R. *J. Solid State Chem.* **1996**, *127*, 87.
(37) Jorgensen, J. D. et al. *Phys. Rev. B* **1988**, *38*, 11337.

CM980221S